IEEE Access
Multidisciplinary | Rapid Review | Open Access Journal

Date of publication xxxx 00, 0000, date of current version xxxx 00, 0000.

Digital Object Identifier 10.1109/ACCESS.2017.DOI

Post-processing of NWP forecasts using Kalman filtering with operational constraints for day-ahead solar power forecasting in Thailand

SUPACHAI SUKSAMOSORN[1], NAEBBOON HOONCHAREON[1] (Member, IEEE), and JITKOMUT SONGSIRI[1] (Member, IEEE)

[1]Smart Grid Research Unit, Department of Electrical Engineering, Faculty of Engineering, Chulalongkorn University, Bangkok, Thailand 10330. (email: suppachai12344@gmail.com, naebboon.h@chula.ac.th, jitkomut.s@chula.ac.th)

Corresponding author: Jitkomut Songsiri (e-mail: jitkomut.s@chula.ac.th)

This work was supported in part by the National Research Council of Thailand Fund on Renewable Energy Framework and by the Research Assistant Scholarship from Graduate School, Chulalongkorn University.

ABSTRACT Solar power forecasting with a day-ahead horizon has played an important role in the operational planning of generating units in power system operations. We aim to develop a solar power forecasting model suitable for a tropical climate, using Thailand as a model, and hence present a linear recursive regression model as a post-processing step for reducing the errors obtained from the Weather Research and Forecasting (WRF) model. This model consists of submodels, each of which predicts the solar irradiance of a particular time of the day. By using a stepwise regression method, we found that WRF forecasts of irradiance, temperature, relative humidity and the solar zenith angle were selected as highly relevant inputs of the model. The regression model coefficients are updated according to a Kalman filtering (KF) scheme so that the model can flexibly adapt to fluctuations in the solar irradiance. We then modify the KF update formula to accommodate the limitation in measurement availability at the time of executing the forecasts. The proposed KF formula can be generalized to find the optimal prediction given that the available measurements are mapped by an affine transformation. The obtained results using actual data from a solar rooftop system located in the central region of Thailand showed that the normalized root-mean-square error (NRMSE) of the solar power was about 12-13% and this was decreased from the NRMSE of the WRF model by 7-12% on average. This improvement was the best out of similar post-processing steps based on the model output statistics framework.

INDEX TERMS Solar irradiance forecasting, Numerical weather prediction, WRF, Kalman filter, model output statistics

I. INTRODUCTION

RECENT renewable energy research has focused on the techniques of solar power forecasting to enhance the power system reliability performance through a smart-grid energy management system. Forecasting specifications can vary upon different temporal horizons, which are related to and are important for the different power system operations [1], [2]. Our primary focus is on the one-day-ahead horizon because of its usage for planning and unit commitment, as one of the current goals of the Electricity Generating Authority of Thailand (EGAT). The review [1] has described all the essential elements of forecasting methods and common techniques, including statistical methods, machine learning, numerical weather prediction (NWP), and hybrid methods [1], [3], [4]. In addition, recent review [2] also provided an economic assessment and specified common techniques with required inputs for each forecasting temporal horizon. Several studies have concluded that NWP forecasts are more beneficial and more accurate than using cloud information from satellites for longer time horizons (15–240 h in advance) [1], [2], [5], [6]. For this reason, the widely-used methods for day-ahead forecasting have mainly included a

combination of NWP (as the main model) with statistical methods or machine learning.

The NWP models solve partial differential equations that explain the model dynamics of Earth's atmosphere and predict involved weather variables. The models can be divided into two categories. The first are global models which run on a global domain such as GFS (Global Forecast System), while the second is a regional model that forecasts only a spatial subdomain [1]. Recent regional models have been developed by different countries, one of which is the Weather Research and Forecasting (WRF) model, available in public domain [7]. Its specific configuration and design for solar energy forecasting was upgraded to WRF-Solar by including representation of aerosol-cloud-radiation systems and implementing more efficient numerical approaches [8], [9]. For solar power forecasting purposes, NWP models can be used to predict the solar irradiance (I) from one hour up to several days ahead with accuracy that varies upon the NWP schemes, grid sizes, and horizons. Various NWP models with multi-day horizons were previously evaluated on locations in the U.S. [10], where, in particular, the root-mean-square error (RMSE) of next-day irradiance prediction from the WRF model ranged from 107–173 $\mathrm{W/m^2}$, depending on the climate conditions (arid or humid continental). In southern Spain [11], WRF models predicted 1- to 2-day ahead with the RMSE around 101-188 $\mathrm{W/m^2}$. The NWP models by SolarAnywhere combine forecasts of the sky-cover fraction and yielded yearly RMSE of I in the range of 139–189 $\mathrm{W/m^2}$ [12]. A study of NWP models revealed that they generally bring large positive biases, which could exceed 200 $\mathrm{W/m^2}$ under cloudy conditions in the U.S. [13]. Also, as evidently seen in Singapore, which has the same tropical climate as Thailand, WRF models overestimate I with an RMSE in the range of 240-258 $\mathrm{W/m^2}$ [14].

The large NWP prediction bias can be reduced by applying a forecast enhancement scheme, or a hybrid method that combines two or more existing models to add up the advantages from several schemes, whose final prediction outputs can be I (in-direct approach) or solar power (P; direct approach). When the NWP and another model are employed in the *cascade* sense, the other model is viewed as a post-processing step to improve the NWP forecasts and was found to be a linear model [15], [16], multi-linear adaptive regression splines (MARS) [17], or nonlinear models such as artificial neural network (ANN)/recurrent neural network (RNN) [18]–[23], fuzzy [21], genetic algorithm [24], or support vector machine (SVM) [15], [24]; all of which were shown to significantly reduce the bias from a baseline. Among these works, the reported RMSE of I in the Rome region amounted to 145-149 $\mathrm{W/m^2}$ [18] or in the range of 96–105 $\mathrm{W/m^2}$ [19]. As a comparative study, NWP outputs were used as predictors for several statistical models including linear regression, generalized additive model, binary trees, random forest, and SVM [15]. The best model of predicting solar power was the random forest that had at least a one-third lower error than that of the baselines.

Integrating a model with NWP can also be employed as a *bias correction* scheme. For this, let $\hat{y}_{\mathrm{nwp}}$ be an NWP prediction of y with a residual error e, expressed by $y = \hat{y}_{\mathrm{nwp}} + e$. A new residual can be better corrected via $\hat{e}_1 = Ge$, where G is a model designed for characterizing the unexplained solar dynamics that remains in e. The final prediction is then given by $\hat{y} = \hat{y}_{\mathrm{nwp}} + \hat{e}_1$. Previous studies have applied the bias correction approach using G as a linear model [25] with the solar zenith angle and the clear sky index as predictors, or G can be nonlinear such as ANN or wavelets [26], [27].

These post-processing steps for improving NWP forecasts are also known as *model output statistics (MOS)*, as initially proposed in the context of weather predictions [28] as a linear regression. As an extension, the regression coefficients can also be recursively estimated to fit best with recent measurement. This scheme was previously implemented using Kalman filtering (KF) to remove the bias, which obeys a linear equation explained by various predictors such as the Global Environmental Multiscale (GEM) model's forecasts [29] or the set of WRF forecasts and solar zenith angle [30]. The KF scheme, denoted as MOS+KF, reduced the RMSE of I from NWP by around 38-40% in Reunion Island [30] and by around 11-23% in Canada [29]. In [31], [32], a dynamic MOS was applied to several NWP models whose coefficient weights were adjusted to deliver an integrated NWP forecast; this blended output was further used with the observed data to perform a forward error correction. The whole process constitutes the DICast methodology as the main day-ahead irradiance forecasting in the operational Kuwait Renewable Energy Prediction System.

Previously mentioned post-processing methods were deterministic frameworks that provided point forecasts, but improving NWP can also be performed with probabilistic frameworks that also bring more information about distribution or uncertainty of forecast values. A few examples of techniques in probabilistic forecasting were quantile gradient boosting [33] and analog ensemble (AnEn) [34], [35]; the AnEn used DICast forecast results as the input to forecast solar power in [31], [32].

Although the aforementioned studies presented several techniques of day-ahead forecasting applied to various climate conditions, further research is still required to explore suitable frameworks for other locations, including Thailand. The first goal of this study was to identify the important weather variables to solar irradiance using a statistical framework and compare this with the literature. The second goal was to develop a forecasting model that provide point forecasts and can be conveniently incorporated into a unit commitment program run by the Short-term Operation Planning Section (SOPS) under the Generation Operation Planning Department of EGAT. In this case, the unit commitment program requires daily predictions of the next-day P during 7:00–16:00 h, to be readily available by 13:00 h of the current date. To the best of our knowledge, the previous studies did not take this practical constraint into account and some complications are introduced due to limited resources of

This article has been accepted for publication in a future issue of this journal, but has not been fully edited. Content may change prior to final publication. Citation information: DOI 10.1109/ACCESS.2021.3099481, IEEE Access

local measurements at the time of forecasting. This paper's contribution is to present forecasting models by engaging practical implementation concerns in the modeling process.

The proposed model consists of 10 MOS+KF submodels, each of which forecasts I of each hour during the day. The inputs of all submodels are selected by partial correlation, stepwise regression, and subset regression analyses. In the forecasting procedure, the model requires the measured data to update the model parameter in a daily manner. As an operational constraint, the predicted P of the next day must be released by 13.00 h, while the ground measurement or any model inputs obtained after 13:00 h are still not available. We then modify the equations of the KF for updating the parameters in the minimum-mean-square sense using only the existing data. The best forecast I is the conditional mean of the next-day I given the information up to present. After the day-head forecasts of I are obtained, we apply a linear photovoltaic (PV) conversion model to estimate the P using the forecasted I.

The proposed forecasting scheme is presented in Section III, while the background on the MOS+KF is presented in Appendix A and our analytical results on the modified KF are in Appendix B. The experimental results evaluated on data collected from lab-scale solar stations are illustrated in Section IV.

II. FORECASTING SPECIFICATIONS

A. PROBLEM STATEMENT

This work aims to predict the PV power (P) one day in advance to help improve the generation scheduling performance of the SOPS in anticipation of a high penetration of PV generation. The SOPS usually starts to plan the generation for the next day after 13:00 h. Suppose d is a day index and t is an hour index during the day. Then t_f was denoted as the forecasting time (the time that forecasts must be released), specified by users, and is 13:00 h in this study. Our forecasting model must provide hourly forecasted P of day $d+1$ between 7:00 to 16:00 by t_f of day d. The available inputs for the proposed model are the (i) meteorological forecasts from NWP (I, temperature (T), relative humidity (RH)), (ii) ground measurements from weather stations acquired up to time t_f (I,T,RH,wind speed (WS)) and (iii) other deterministic variables such as the solar zenith angle ($\cos\theta$) or clear-sky irradiance (I_{clr}). Based on the existing computation resources and a pre-analysis of our NWP implementation in Section II-B, a scheme of improving NWP forecasts of I using the available inputs must be executed during 3:00 to 13:00 h of day d.

B. THE WRF DATA

Next-day weather forecasts are influential inputs for a day-ahead forecasting model as I highly depends on meteorological variables, whose forecasts are commonly obtained from an NWP model [1], [2]. The NWP model used in this study was the WRF model, developed and maintained as a community model by the National Center for Atmospheric Research [7]. The WRF model requires initial and lateral boundary conditions which can be obtained from global or regional models with a domain that emcompasses the WRF domain. In this work, we used the GFS (global model) provided by the National Oceanic and Atmospheric Administration. The WRF outputs used in this study were the predicted T, RH and I (global horizontal irradiance or GHI, namely SWDOWN from WRF output). Fig. 1 shows the first spatial domain set in WRF with a grid spacing of 9×9 km^2 that covered the western, central and eastern regions of Thailand, while the second domain (3×3 km^2) focused on central Thailand. The temporal resolution of one-day-ahead WRF forecasts was one hour. The Weather Forecast Bureau of the Thai Meteorological Department (TMD) suggested the WRF physics parameterizations in Table 1 which generally worked well for weather forecasting in Thailand (private communication, Aug 2017).

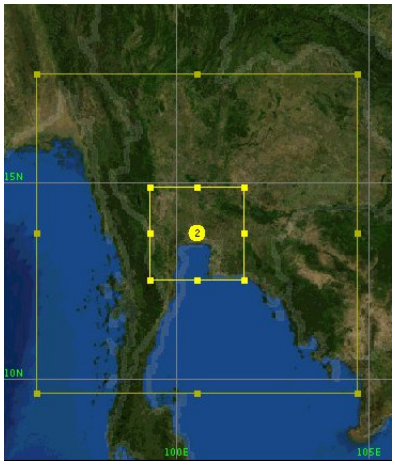

FIGURE 1: The two domains of WRF with grid spacing of 9×9 km^2 and 3×3 km^2. The two solar sites are located at the center of the second domain with the latitude and longitude of (13.737 N,100.532 E).

TABLE 1: Physics options set in the WRF model [36, §5].

Physics options	Schemes
Micro physics options	WRF Single–moment six–class Scheme
Planetary boundary layer physics options	Mellor–Yamada Nakanishi Niino (MYNN) Level 2.5 Scheme
Cumulus parameterization options	Grell 3D scheme
Shortwave and longwave options	RRTMG shortwave and longwave schemes [37]
Land surface options	Unified Noah land surface model
Surface layer options	Revised MM5 scheme

Time constraint. From Fig. 2a, the GFS model was run daily at 0:00, 6:00, 12.00, and 18.00 h Universal Time Coordinated (UTC), or at 7:00, 13:00, 19:00, and 1:00 h Thailand Standard Time (TST) and marked in blue dots. The GFS model takes 4 h to run the entire forecast, so the input data for the WRF were available to download at 11:00, 17:00, 23:00, 5:00 h TST (shown in green dots). Our PC (CPU: Intel®Xeon®Processor E5-2620 v4 2.10GHz 8 Cores

This article has been accepted for publication in a future issue of this journal, but has not been fully edited. Content may change prior to final publication. Citation information: DOI 10.1109/ACCESS.2021.3099481, IEEE Access

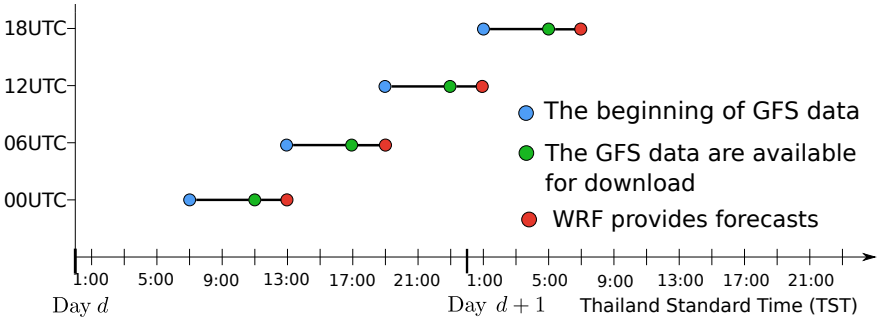

(a) Available options of input data.

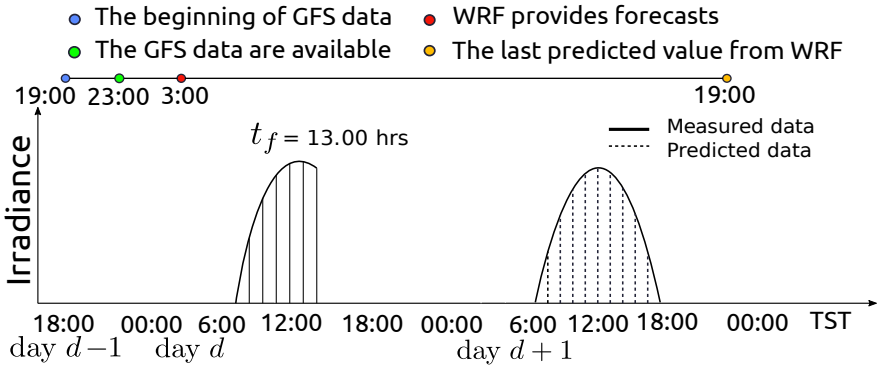

(b) Recommended time schedule by using input of 12UTC.

FIGURE 2: Time schedule of input data in the WRF model.

16 threads 20 MB SmartCache 8 GT/s QPI, DDR4-2400 RAM 32 GB) takes 2 h to compute the one-day-ahead WRF. Therefore, the WRF predictions are available at times marked as red dots in Fig. 2a. It was not possible to obtain the WRF predictions of day $d+1$ by 13:00 h on day d (forecasting time) unless the WRF model was run *two days* in advance.

As such, the WRF model was set to provide two-day-ahead predictions twice, each computation taking 4 h , on day $d-1$, using the GFS inputs of 00:00 h UTC and 12:00 h UTC. The latter time was selected because the resulting forecast of irradiance had a lower error. Our WRF implementation concluded in Fig. 2b indicated the operational specification that the post-processing scheme for improving WRF forecasts must take place during 3:00-13:00 h (TST).

C. MEASUREMENT DATA

The solar measurement data were collected from two rooftop-solar stations (8 kW and 15 kW) and meteorological sensors installed at the Electrical Engineering Building, Chulalongkorn University, Thailand. We used I from the pyranometer and P from the energy meter. Typical preprocessing steps were required to assure the data quality control, including duplicate recordings, missing values, out-of-range values, outliers, and non-updated values. All erroneous records were imputed differently depending on the record length. We applied a linear interpolation to short consecutive records (less than 1h), while for long records (more than 1h), we implemented a moving average with a window covering the previous and the next 10 days of imputed values.

In conclusion, we used measurements of I and P that were downsampled using moving average to hourly format, and used forecasts of $I, \mathrm{T}, \mathrm{RH}$ from the WRF. All data were collected hourly from 7:00–16:00 h (TST) during January 1, 2017 to December 31, 2018. Data during 17:00-18:00 h were excluded due to a shading effect on the building rooftop. The training data set were selected during January 1, 2017 to June 30, 2018 and the test data were from July 1 to December 31, 2018. The ratio of training to test datasets was 3:1.

III. PROPOSED METHOD

Based on previous reviews in [1], [2], [4], [38], there are three main aspects as options to be considered. Firstly, indirect solar power forecasting was performed, where I was predicted and then using a PV power conversion model, the predicted power was obtained. A benefit of the indirect over direct forecasting is that we could characterize forecasting errors from the irradiance forecasting model and power conversion model separately since both measurements of I and P can contain outliers or missing values to different degrees. Another reason is that a good irradiance forecasting model can be readily applied to other solar farm areas, while the process of training PV power conversion models to a specific location does not require much computational effort. Secondly, from the literature of improving NWP forecasts [13], [16], [25],

This article has been accepted for publication in a future issue of this journal, but has not been fully edited. Content may change prior to final publication. Citation information: DOI 10.1109/ACCESS.2021.3099481, IEEE Access

[29], [30], the common input choices of correcting NWP forecasts are $I_{\mathrm{wrf}}, \mathrm{T}_{\mathrm{wrf}}, \mathrm{RH}_{\mathrm{wrf}}$, wind speed ($\mathrm{WS}_{\mathrm{wrf}}$), and deterministic inputs including the clear sky index (k_{wrf}), solar zenith angle ($\cos\theta$), and clear-sky irradiance (I_{clr}). While it is commonly known that these weather variables are correlated with I, a feature selection should be systematically performed on the data sets in this region in order to regard only significant inputs. Thirdly, spatial averaging has become a common post-processing step of NWP forecasts to reduce the errors [13], [29], [39]. From these points of view, we design the whole scheme of solar power forecasting in Fig. 3, where the key result of our paper is the solar irradiance forecasting module as a post-processing step from WRF forecasts using the proposed modified KF scheme to accommodate the operational constraints.

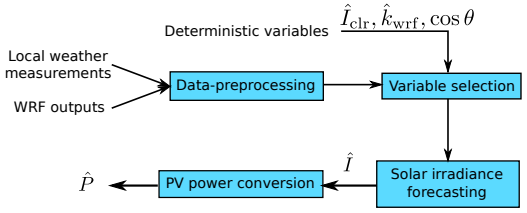

FIGURE 3: Proposed scheme of one-day-ahead PV power forecasting.

A. SPATIAL AVERAGING

It is known that spatial averaging can reduce NWP forecast errors. In [25], the RMSE was reduced by half when using a spatial area of $3^\circ \times 3^\circ$ in the averaging. Our WRF forecasts were computed at a grid spacing of 3×3 km^2. This study applied a spatial averaging of WRF forecasts, given by

$$\hat{I}_{\mathrm{spatial}}(t) = (1/mn) \sum_{i=1}^{m} \sum_{j=1}^{n} \hat{I}_{\mathrm{nwp}}(p_i, q_j)(t), \qquad (1)$$

where $\hat{I}_{\mathrm{wrf}}(p_i, q_j)$ is the predicted I from the WRF model at latitude and longitude coordinates of (p_i, q_j), and t is the time index. We consider using $(m, n) = (3, 3), (5, 5), (7, 7)$ in averaging, which correspond to spatial areas of $6 \times 6, 12 \times 12$, and 18×18 km^2, respectively.

B. VARIABLE SELECTION

We followed the previously reported scheme of variable selection that used partial correlation, stepwise regression, and subset regression [40]. The variables used to perform a significance test on the regression coefficients were $\hat{I}_{\mathrm{wrf}}, \widehat{\mathrm{RH}}_{\mathrm{wrf}}, \hat{\mathrm{T}}_{\mathrm{wrf}}$, $I_{\mathrm{clr}}, \cos\theta$, and $\hat{k}_{\mathrm{wrf}}$ (clear-sky index). Note that we calculated I_{clr} from the Ineichen clear sky model [1] with an estimated Linke turbidity value of 4.8597 for Thailand, using the least-squares (LS) method.

The results in Table 2 were performed on the training data and suggested that $I_{\mathrm{wrf}}, \mathrm{RH}_{\mathrm{wrf}}, \mathrm{T}_{\mathrm{wrf}}$, and $\cos\theta$ were mostly

TABLE 2: Selected weather variables from various methods using the data collected from January 1, 2017 to June 30, 2018.

Method	Predictor variables					
	$\hat{I}_{\mathrm{wrf}}$	$\widehat{\mathrm{RH}}_{\mathrm{wrf}}$	$\hat{\mathrm{T}}_{\mathrm{wrf}}$	I_{clr}	$\cos\theta$	$\hat{k}_{\mathrm{wrf}}$
Partial correlation	•		•		•	
Forward stepwise	•	•	•	•	•	
Backward stepwise	•	•	•	•	•	
Subset regression						
AIC	•	•	•		•	
BIC	•	•	•		•	

selected by all the methods and subsequently used as the predictors of the proposed MOS model, given by

$$\hat{I}_{\mathrm{mos}}(t) = \beta_1 \hat{I}_{\mathrm{wrf}}(t) + \beta_2 \widehat{\mathrm{RH}}_{\mathrm{wrf}}(t) + \beta_3 \hat{\mathrm{T}}_{\mathrm{wrf}}(t) + \beta_4 \cos\theta(t). \qquad (2)$$

Note that the clear-sky index, $\hat{k}_{\mathrm{wrf}} = \hat{I}_{\mathrm{wrf}}/I_{\mathrm{clr}}$ was not selected by any variable selection method due to its dependence on $\hat{I}_{\mathrm{wrf}}$ and I_{clr}. The significance test of regression coefficients in (2) was performed at a significance level of $\alpha = 0.05$ and the results are shown in Table 3, where all of the selected variables were significant in the regression model (2).

TABLE 3: Regression coefficients, standard error, and p-values of the coefficients of the proposed MOS model.

Variables	Unit	Coeff.	SE	p-value
$\hat{I}_{\mathrm{wrf}}(t)$	W/m^2	0.522	0.020	1.545×10^{-137}
$\widehat{\mathrm{RH}}_{\mathrm{wrf}}(t)$	%	0.183	0.190	2.279×10^{-9}
$\hat{\mathrm{T}}_{\mathrm{wrf}}(t)$	°C	-4.280	0.536	1.613×10^{-15}
$\cos\theta(t)$	-	267.84	19.901	1.214×10^{-40}

C. SOLAR IRRADIANCE FORECASTING MODEL

Empirical distributions of the residual errors of spatially averaged WRF irradiance forecasts are shown in Fig. 4. Overall, the WRF model tended to overestimate (shown as significant positive biases during 10:00-16:00 h), which agrees with previous findings [13]. Relatively high degrees of error variations were observed during 11:00 to 14:00 h, while the error was generally smaller in the early morning. These results suggest that an *adaptive* forecasting model should be designed and customized to different bias characteristics for *each hour*.

The proposed forecasting model for I was based on the regression model: $\hat{I}(t) = \beta_1 x_1(t) + \beta_2 x_2(t) + \cdots + \beta_p x_p(t) = x^T \beta$, where $x = (x_1, \ldots, x_p)$ are predictors (the important variables to solar irradiance) and β is the parameter estimated by the least-squares (LS) method. The post-processing step applied the KF to estimate β in an online-manner to compensate for the estimation error when up-to-date measurements of I arrive. This is referred to as MOS in the literature of meteorological forecasting and recursive least-squares (RLS) in estimation. This approach starts with assuming that β , regarded as a state variable, obeys a random walk equation,

This article has been accepted for publication in a future issue of this journal, but has not been fully edited. Content may change prior to final publication. Citation information: DOI 10.1109/ACCESS.2021.3099481, IEEE Access

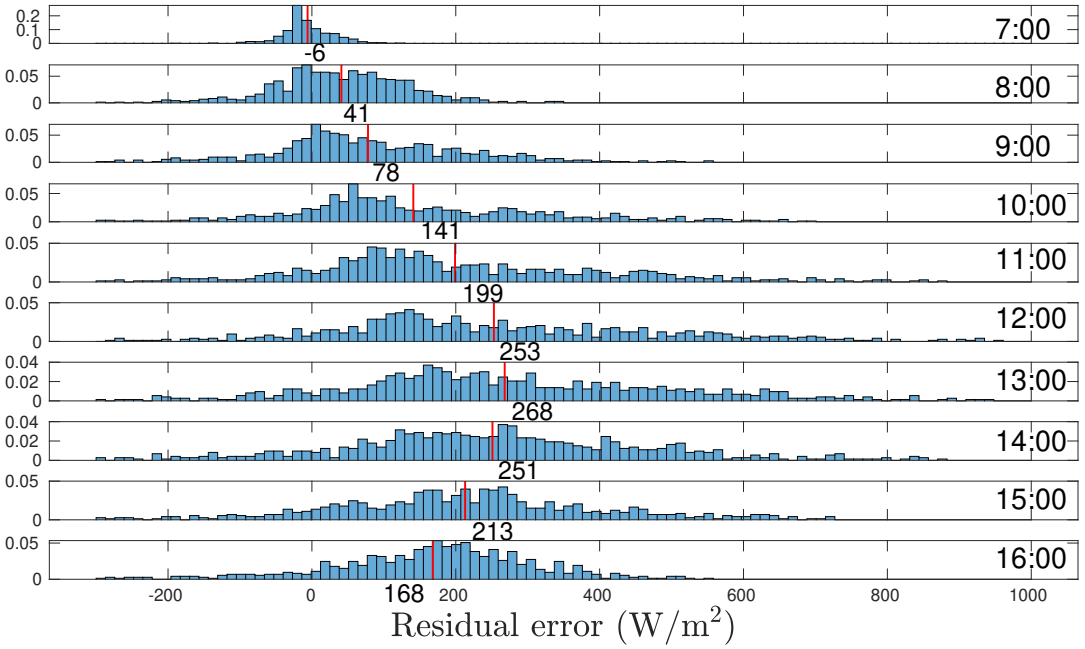

FIGURE 4: Histogram of residual errors of the predicted solar irradiance from the WRF model, collected at various hours of the day. The red lines are the mean of error.

where $I(t)$ is the output of a state-space system. A detailed background is given in Appendix A.

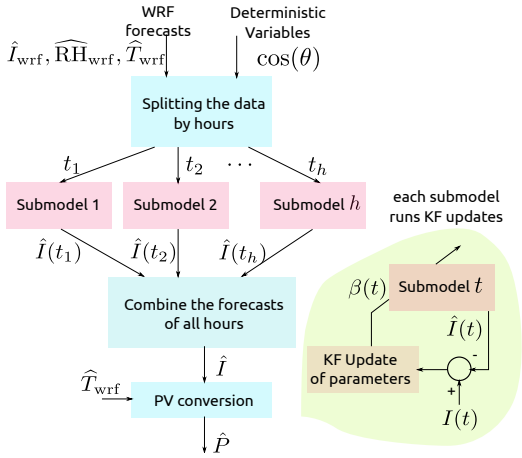

FIGURE 5: The daily-step irradiance forecasting model.

As empirical distributions of WRF are biased depending upon the time (Fig. 4), our main forecasting model was proposed to consist of h submodels, each forecasting I of a specific hour (*i.e.*, submodels 1,2,…, h predicts I at 7:00, 8:00,…, 16:00 h, respectively, where $h = 10$) and the scheme is presented in Fig. 5. From this setting, $\beta(t)$ refers to the regression coefficient of a submodel of hour t, for $t \in \{t_1, t_2, \ldots, t_h\} = \{7{:}00, 8{:}00, \ldots, 16{:}00\text{ h}\}$. The forecasting scheme at t_f starts with collecting model inputs (WRF forecasts and solar zenith angle of the next day) and then splits these inputs into different hours. Each submodel t takes the corresponding inputs to produce the next-day $\hat{I}$ of time t in parallel. Consequently, the irradiance forecasts of all hours are merged and converted to the predicted power. Each submodel also runs KF to update its parameters by taking the bias as the correction input.

In Appendix A, we mentioned that the KF update can be run either in hourly or daily steps. As we aimed for a day-ahead forecasting and each hour-specific submodel has its own parameter, our assumption in applying KF was that $\beta(t)$ should *evolve daily*, *i.e.*, the parameter of today should be adjusted from yesterday's value when the new measurement is observed. Hence, the model is proposed as a *daily-step* model and consists of the state-space equations: for $t = t_1, \ldots, t_h$ as shown in (3)-(4):

$$\beta^{(d+1)}(t) = \beta^{(d)}(t) + w^{(d)}(t), \tag{3}$$

$$I^{(d)}(t) = C^{(d)}(t)\beta^{(d)}(t) + v^{(d)}(t), \tag{4}$$

where the output matrix, defined from the MOS model (2) is

$$C^{(d)}(t) = \left[\hat{I}^{(d)}_{\text{wrf}}(t) \quad \widehat{\text{RH}}^{(d)}_{\text{wrf}}(t) \quad \widehat{\text{T}}^{(d)}_{\text{wrf}}(t) \quad \cos\theta(t)^{(d)}\right]. \tag{5}$$

Our notation of $z^{(d)}(t)$ is the variable of day d at hour $t \in \{t_1, \ldots, t_h\}$, so the system (3) and (4) progresses as $d = 0, 1, \ldots,$ for each fixed hour. In the context of a stochastic state-space system, w and v are the state and measurement noises whose covariance matrices are required when applying the KF.

As mentioned previously, we proposed a modified KF scheme to update the parameters before t_f=13:00 h when some measurements of I are not available. It is more compactly unified to explain this idea by combining all h submodel equations as a single vector equation. If we

This article has been accepted for publication in a future issue of this journal, but has not been fully edited. Content may change prior to final publication. Citation information: DOI 10.1109/ACCESS.2021.3099481, IEEE Access

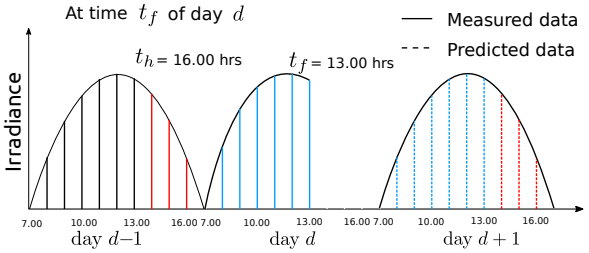

(a) At time t_f of day d, we update the model parameters of 7:00-13:00 h (blue lines) using available measurements. The parameters of 14:00-16:00 h (red lines) were updated on day $d-1$ and held to day d. Parameters of all submodels are used for the prediction of day $d+1$.

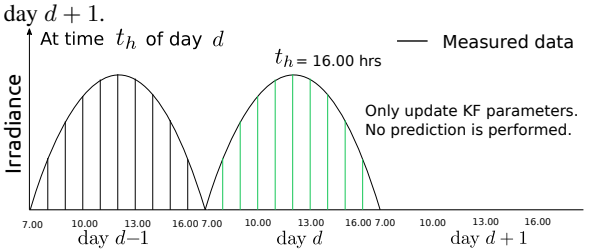

(b) At time t_h of day d, measurements of 14:00-16:00 h are available; hence, the measurements of all hours are complete, denoted by the green lines. All submodels' parameters can be updated using the conventional KF routine and will be used for the next day at time t_f. No forecasts are released at t_h of day d.

FIGURE 6: Updating time of the parameters in Kalman filter.

define $z^{(d+1)} = (\beta^{(d+1)}(t_1), \ldots, \beta^{(d+1)}(t_h))$ and $y^{(d)} = (I^{(d)}(t_1), \ldots, I^{(d)}(t_h))$ then all h models in (3) and (4) can be grouped in a single state-space system as

$$z^{(d+1)} = Az^{(d)} + w^{(d)}, \quad y^{(d)} = C^{(d)}z^{(d)} + v^{(d)}, \qquad (6)$$

where $z^{(d)} \in \mathbf{R}^{ph}, y^{(d)} \in \mathbf{R}^{h}$, $A = I_{ph}$ (identity matrix of size ph) and $C^{(d)}$ is block-diagonal, given by $\mathbf{diag}(C^{(d)}(t_1), C^{(d)}(t_2), \ldots, C^{(d)}(t_h))$. In a KF context, denote $\hat{z}^{(d+1|d)}$ as the state estimate of day $d+1$ using the past information up to day d, $K^{(d)}$ is the Kalman gain of day d, and $P^{(d+1|d)} = \mathbf{E}[(z^{(d+1)} - \hat{z}^{(d+1|d)})(z^{(d+1)} - \hat{z}^{(d+1|d)})^T]$ is the corresponding covariance of the state estimation error. Moreover, W and V are covariances of $w^{(d)}$ and $v^{(d)}$, respectively. In a conventional KF [41], when A is identity and $C^{(d)}, W, V, P^{(0|0)}$ are block diagonal, then $K^{(d)}, P^{(d|d)}$, and $P^{(d|d-1)}$ are also block diagonal matrices. Therefore, $\hat{z}^{(d|d)}$ and $\hat{z}^{(d+1|d)}$ can be updated in parallel for each t. The details of the initial parameters and noise covariances are given in Appendix C.

Modification of KF. From the forecasting specification in Section II, the predicted P of the next day must be provided by $t_f = 13.00$ h of each day, so the measurements during 13:00-16:00 h are not available. KF scheme can only use the available chunk of measurements, cast as $Fy^{(d)}$ where $F = \begin{bmatrix} I_r & 0_{r\times(h-r)} \end{bmatrix}$ and r is the number of hours between t_1 and t_f. To deal with this practical constraint, we applied the result of Proposition 1 in Appendix B, which explains how the optimal estimator in the KF scheme should be modified when the measurement is transformed by a general matrix F. The modified KF iteration at t_f is as follows.

Measurement update at t_f:

$$\begin{aligned} K^{(d)} &= P^{(d|d-1)}(C^{(d)})^T F^T \\ &\quad \times \left[FC^{(d)}P^{(d|d-1)}(C^{(d)})^T F^T + FVF^T\right]^{-1}, \\ \hat{z}^{(d|d)} &= \hat{z}^{(d|d-1)} + K^{(d)}(Fy^{(d)} - FC^{(d)}\hat{x}^{(d|d-1)}), \\ P^{(d|d)} &= (I - K^{(d)}FC^{(d)})P^{(d|d-1)}. \end{aligned}$$

If $A = I$, $P^{(d|d-1)}$ is initialized by a diagonal matrix, and $C^{(d)}$ is block diagonal, then we can show that the last $h-r$ rows of $K^{(d)}$ are zero, which implies that the coefficients $\beta^{(d)}(t)$ associated with $t > t_f$ are not updated.

Time update at t_f:

$$\hat{z}^{(d+1|d)} = A\hat{z}^{(d|d)}, \quad P^{(d+1|d)} = AP^{(d|d)}A^T + W.$$

The output of the KF scheme is the next-day forecasted I, given by $\hat{I}^{(d+1)} = \hat{y}^{(d+1)} = C^{(d+1)}\hat{z}^{(d+1|d)}(t)$ for $t \in \{t_1, t_2, \ldots, t_h\}$ where $C^{(d+1)}$ contains the WRF predictions of day $d+1$ as stated in (5). For details, the KF state estimates of $t \in \{t_1, t_2, \ldots, t_f\}$ are updated and are used to predict I as blue lines in Fig. 6a. The KF state estimates of $t \in \{t_f+1, t_f+2, \ldots, t_h\}$ are not updated and are held from the value of day $d-1$ at time t_h as the red line in Fig. 6a. At time t_h of day d, the local measurements can all be collected as the green line in Fig. 6b. We then updated the KF again using the regular procedure. All submodels' parameters are updated but no forecasts are delivered out at this stage.

D. PV POWER CONVERSION MODEL

From a review of PV cells in [42, §3.5], the solar power can be estimated instantly from the solar irradiance and cell temperature, guiding us to use a static conversion model expressed by $P(t) = \beta_1 I(t) + \beta_2 \mathrm{T}(t) + \beta_3 I(t) \cdot \mathrm{T}(t)$. For solar power prediction of day $d+1$, all the terms on the right hand side are replaced with the predictions of day $d+1$ as

$$\begin{aligned} \hat{P}^{(d+1)}(t) = \beta_1 \hat{I}^{(d+1)}(t) + \beta_2 \hat{\mathrm{T}}^{(d+1)}_{\mathrm{wrf}}(t) \\ + \beta_3 \hat{I}^{(d+1)}(t) \cdot \hat{\mathrm{T}}^{(d+1)}_{\mathrm{wrf}}(t), \end{aligned} \qquad (7)$$

where $(\beta_1, \beta_2, \beta_3)$ can be estimated from the linear regression method using historical data.

IV. PERFORMANCE EVALUATION

This section presents the forecasting performance of the WRF model and the improvement obtained by the proposed method. The residual error is defined as $\hat{y} - y$ (prediction-measurement), so the model overestimates if the averaged residual error is positive. We consider common performance indices including RMSE, mean-bias error (MBE), mean absolute error (MAE) and their normalization counterparts: NRMSE, NMBE and NMAE using the installed capacity of the two solar power sites as the normalization factor. Reported results and computer codes are available at https://github.com/jitkomut/solarnwpmos.

This article has been accepted for publication in a future issue of this journal, but has not been fully edited. Content may change prior to final publication. Citation information: DOI 10.1109/ACCESS.2021.3099481, IEEE Access

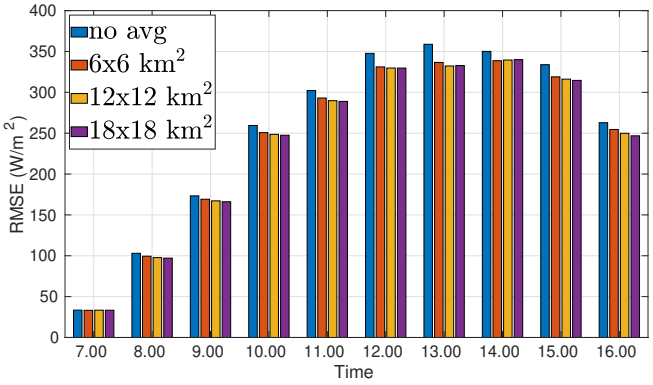

FIGURE 7: The RMSE of the spatial average of predicted solar irradiance from WRF under various areas. The RMSEs (averaged over all samples) after spatial averaging are 274.42W/m^2 (no averaging), 263.15 W/m^2 (6x6 km^2), 260.99 W/m^2 (12x12km^3), and 260.34 W/m^2 (18x18 km^2).

A. THE WRF PREDICTIONS

Since a solar site typically is not located on an exact grid of WRF forecasts, one can choose the nearest grid point to represent the prediction of a point of interest. Performing a spatial averaging (1) over the areas of 6×6, 12×12, and 18×18 km^2, we observed a decreasing trend of RMSE as the area increased in Fig. 7, consistent with [25]. Thus, we used the spatially-averaged WRF forecasts on the area of 18×18 km^2 instead of the forecasts on the single nearest grid point.

B. SOLAR POWER FORECASTING

We consider a persistence model as a baseline and MOS-based methods in the literature to be compared with our irradiance forecasting model. Applying the PV model in Section III-D, we obtained the predicted P converted from the predicted I from the following models.

- Persistence irradiance model produces the forecasts of day $d+1$: $\hat{I}(t) = k(t) I_{\text{clr}}(t)$ for all t. If $t \le t_f$, the clear-sky index $k(t)$ is computed from the measured I of day d; otherwise, $k(t)$ is computed from $\hat{I}_{\text{wrf}}(t)$ of day d.
- Lorenz [25] applied MOS as a bias correction by regressing WRF biases ($\hat{I}_{\text{wrf}} - I$) on the 4$^{\text{th}}$-order polynomial of $\cos\theta(t)$ and $k(t)$. The prediction was then $\hat{I}_{\text{lorenz}} = \hat{I}_{\text{wrf}} + \widehat{\text{Bias}}$ and denoted as MOS$_{\text{lorenz}}$.
- Pelland [29] produced forecasts for 0 to 2-day-ahead horizons by performing a bias correction with KF that updated parameters in an *hourly* step. The bias was regressed on $\hat{I}_{\text{wrf}}$ and the prediction was $\hat{I}_{\text{pelland}} = \hat{I}_{\text{wrf}} + \widehat{\text{Bias}}$, denoted as KF$_{\text{pelland}}$. The noise covariances were frequently updated from sample errors.
- Diagne [30] developed an hour-ahead forecasting model, applying the same hourly KF scheme as [29] but the bias was regressed on $\hat{I}_{\text{wrf}}$ and $\cos\theta(t)$ and the noise covariances were $V = 0.01$, and $W = I$. The prediction was $\hat{I}_{\text{diagne}} = \hat{I}_{\text{wrf}} + \widehat{\text{Bias}}$ and denoted as KF$_{\text{diagne}}$.

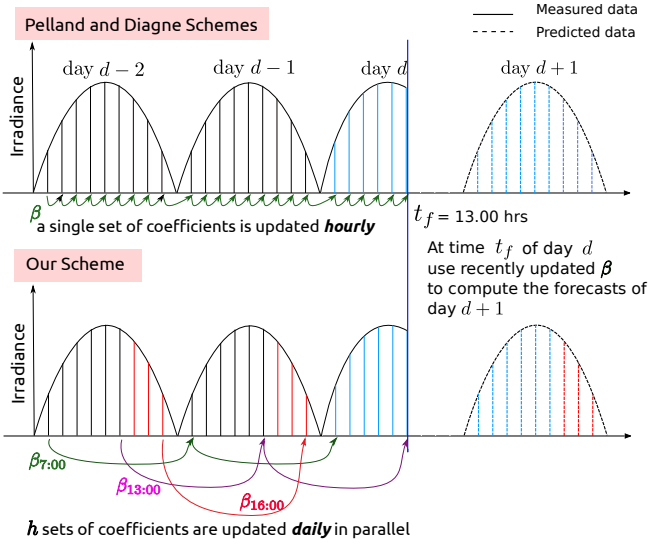

FIGURE 8: Comparison of KF update schemes between our method and those in the literature. At time t_f of day d, measurements corresponding to blue lines are used to update the model parameters and compute the forecasts. For our scheme, the submodel parameters of 14:00-16:00 h are held from the updates on day $d-1$ (red lines).

The main differences between our KF model, denoted as KF$_{\text{daily}}$ and the KF schemes of Pelland and Diagne, illustrated in Fig. 8, are that (i) both of their models contained a single set of regression coefficient β, while our model has h sets of β, each corresponding to submodel parameters, and (ii) their KF schemes update β in hourly format, while our approach updates β of each submodel in a daily manner. Both KF$_{\text{pelland}}$ and KF$_{\text{diagne}}$ rely on the regression model with the output as Bias $= \hat{I}_{\text{wrf}} - I$, then at the forecasting time t_f, the parameters updated from the previous *hour* are held and used to compensate for the predicted bias. Although KF$_{\text{diagne}}$ was originally intended for an hour-ahead forecasting, its implementation for the day-ahead forecasting in our study can suggest if the hourly update scheme and the choice of predictors and KF parameter settings are suitable for a day-ahead forecasting purpose.

We are also aware of other post-processing schemes using complex nonlinear models, such as neural networks in the recent literature. However, we limit our comparison to be among linear recursive models using a KF scheme because of its structural simplicity and that the additional feature of updating parameters can be an advantage over complex models. In the implementation of the method listed above, we used the same parameter setting, known to affect the performance, as in the reference. Potential factors influencing the forecasting accuracy of models are the (i) influential variables included in the model, (ii) model structure, and (iii) KF parameter settings such as noise covariances.

Fig. 9 shows the RMSE and MBE of I versus hour of the day. All forecasting methods yielded the same trends of

This article has been accepted for publication in a future issue of this journal, but has not been fully edited. Content may change prior to final publication. Citation information: DOI 10.1109/ACCESS.2021.3099481, IEEE Access

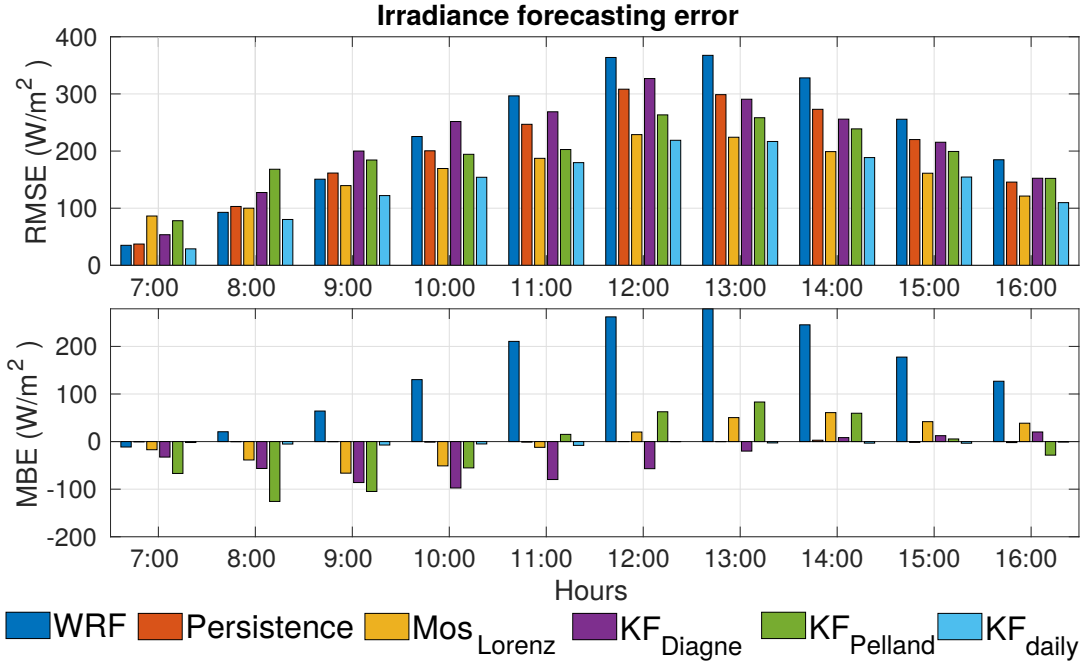

FIGURE 9: **Solar irradiance** forecasting performance.

TABLE 4: The regression coefficients of PV conversion models (7) for 8 kW and 15 kW PV systems. The output is the predicted power (kW).

PV site	Regression coefficient of the predictor		
	$\hat{I}_{\mathrm{wrf}}$ (kW/m^2)	$\hat{\mathrm{T}}_{\mathrm{wrf}}$ (°C)	$\hat{I}_{\mathrm{wrf}}\hat{\mathrm{T}}_{\mathrm{wrf}}$
8 kW	9.4451	−0.0031	−0.0929
15 kW	17.9051	−0.0226	−1.4267

errors that are generally high during 12:00-14:00 h due to a high degree of fluctuation in weather conditions. Clearly from the MBE plot, the WRF model yielded positive biases and hence overestimated. After 10:00 h, the naive persistence model reduced the RMSE from WRF by 11–21% (computed as the improved RMSE relative to the RMSE of WRF), $\mathrm{MOS}_{\mathrm{lorenz}}$ was improved from the WRF by 24–39% and our method greatly reduced the RMSE by 31–42%. As recursive estimations, the Diagne and Pelland methods unexpectedly did not perform as well as the (non-recursive) Lorenz model, implying that it may be due to the parameter setting in their KF schemes. The state noise covariance, W, known to influence the adaptation rate of parameters and set as $W = I$ in [30], was too high for our day-ahead forecasting using this dataset. Unsatisfactory results of the Pelland model [29] can be explained from the online estimates of W and V that resulted in too frequent changes of the model parameters. Our method outperformed the Lorenz model because of our KF scheme of updating model parameters and the choice of model inputs. While we selected the variables in (2) using a statistical method that favors independent variables, highly correlated with I, the Lorenz model used only the solar zenith angle, but not other weather variables.

The ratio of $\hat{I}_{\mathrm{wrf}}$'s coefficient shown in Table 4 to the installed capacity is around 1.18–1.19 (area^{-1}) for the two solar sites. Hence, a benefit of using a simple linear conversion model is that in other areas, we can use this ratio factor to estimate the potentially generated power if the area is known. The hourly accuracy of solar power prediction in Fig. 10 indicates that our method achieved the best performance in all hours, similar to the irradiance forecasting results.

The averaged accuracy (over all hours) are shown in Table 5. Our method achieved the lowest RMSE in irradiance prediction of 156 W/m^2 and the lowest NRMSE of 12.7% and 13.7% in solar power prediction. These are significant reductions (by around 8%) from the NRMSE of WRF power forecasts. The second best model, in terms of RMSE and MAE was the adjusted Diagne model, obtained by reducing the covariance W required in the KF update from I to $10^{-5}I$. This supported our hypothesis that even though Diagne's model was intended for an hour-ahead forecasting, its bias correction and KF schemes are interesting to be compared with, while tweaking W from their original value is needed to obtain a suitable frequency update of the day-ahead model. Our method can further reduce the NRMSE and NMAE of P from the adjusted Diagne model by around 0.7% and 0.45 %, respectively. As for MBE, our method did not achieve the least averaged bias in all cases but the values were in a comparable range. The p-values of the Wilcoxon signed rank test shown in Appendix D suggest that our method yielded significant improvements of irradiance RMSE and MAE (except MBE), over all the other compared models.

An example of time series plots of the predicted P of the 8 kW station is shown in Fig. 11. We selected the 10 days of lowest (and highest) daily-averaged RMSE from our method

This article has been accepted for publication in a future issue of this journal, but has not been fully edited. Content may change prior to final publication. Citation information: DOI 10.1109/ACCESS.2021.3099481, IEEE Access

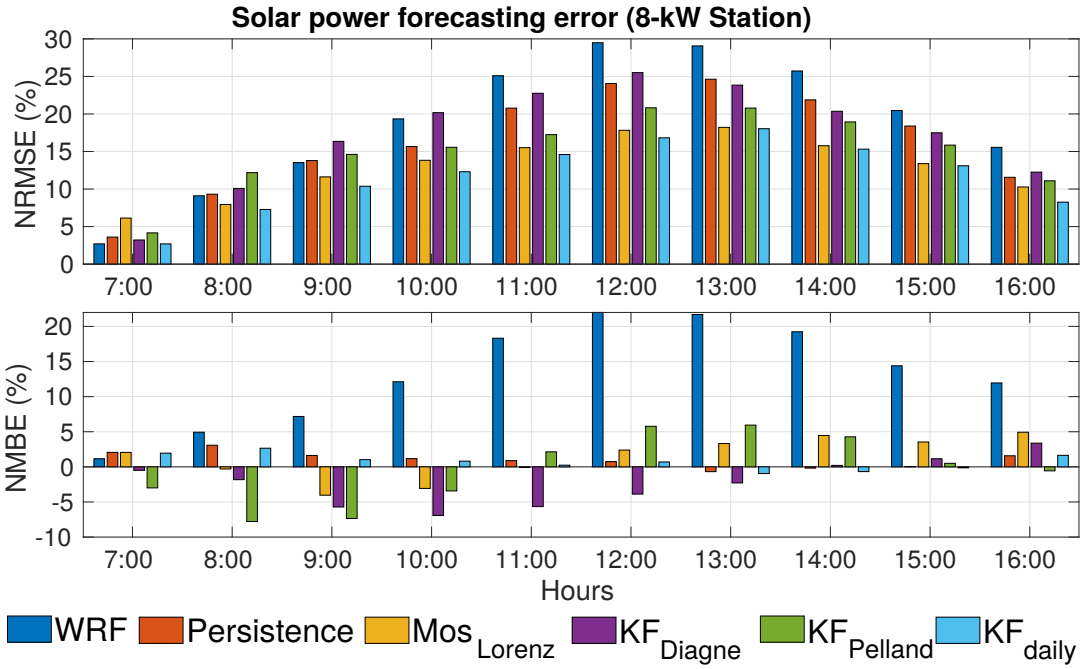

(a) 8-kW Solar station.

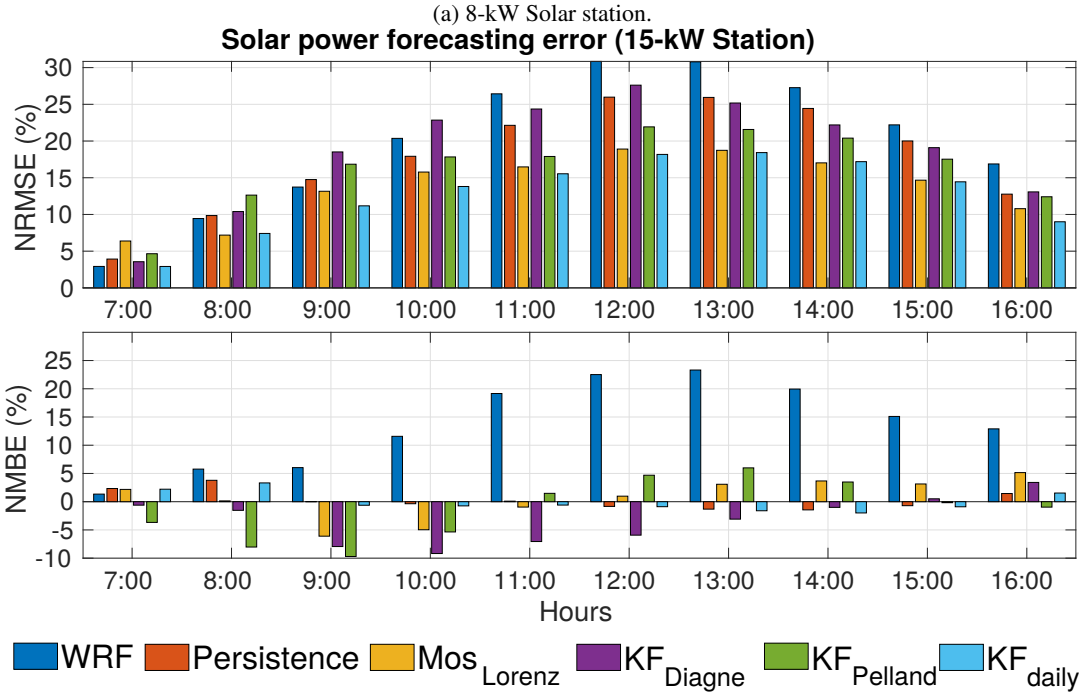

(b) 15-kW Solar station.

FIGURE 10: **Solar power** forecasting performance.

This article has been accepted for publication in a future issue of this journal, but has not been fully edited. Content may change prior to final publication. Citation information: DOI 10.1109/ACCESS.2021.3099481, IEEE Access

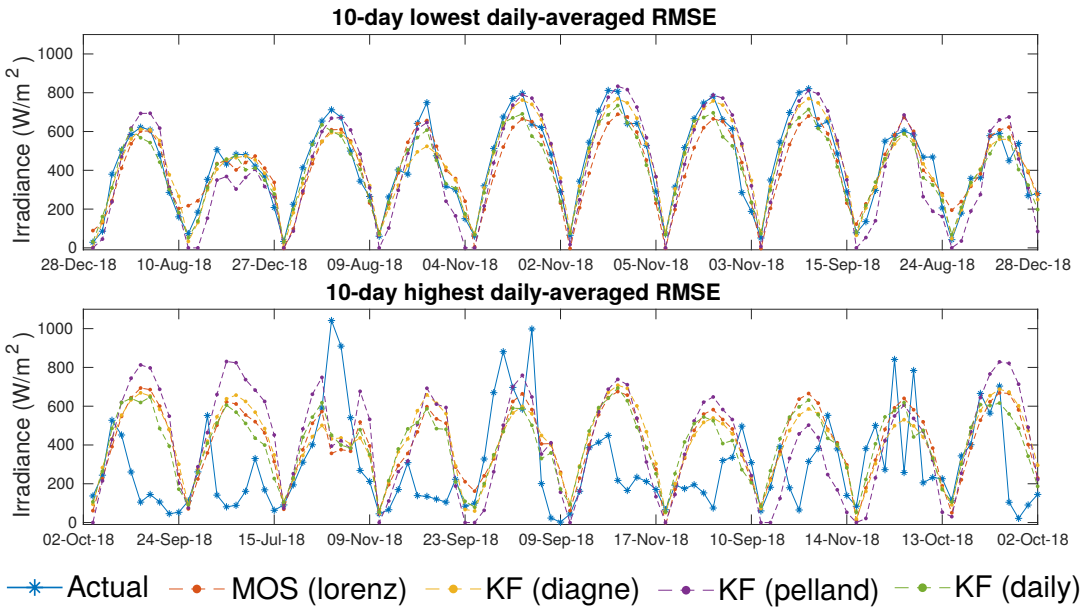

FIGURE 11: Examples of predicted solar irradiance.

TABLE 5: **Solar power** forecasting performances. The RMSE, MAE and MBE of I in % are normalized by the averaged GHI of $393.2\mathrm{W/m}^2$. The NRMSE, NMAE and NMBE of P are normalized by the plant capacity.

Method	**RMSE (W/m^2)** (Irradiance)	**NRMSE (%)** (Power,8 kW)	**NRMSE (%)** (Power,15 kW)
WRF	254.14 (64.79 %)	20.77	21.95
Persistence	216.28 (55.14 %)	17.61	19.10
Lorenz	168.43 (42.94 %)	13.60	14.55
Diagne	228.30 (58.20 %)	18.42	20.01
Diagne (adjusted)	166.66 (42.49 %)	13.39	14.48
Pelland	200.81 (51.20 %)	15.87	17.11
KF (daily)	**156.42 (39.88 %)**	**12.71**	**13.70**
Method	**MAE (W/m^2)** (Irradiance)	**NMAE (%)** (Power,8 kW)	**NMAE (%)** (Power,15 kW)
WRF	186.52 (47.55 %)	15.39	16.20
Persistence	154.53 (39.40 %)	12.69	13.93
Lorenz	134.95 (34.40 %)	10.89	11.53
Diagne	167.08 (42.60 %)	13.40	14.62
Diagne (adjusted)	128.24 (32.69 %)	10.18	11.13
Pelland	155.94 (39.76 %)	12.15	13.15
KF (daily)	**120.44 (30.71 %)**	**9.83**	**10.68**
Method	**MBE (W/m^2)** (Irradiance)	**NMBE (%)** (Power,8 kW)	**NMBE (%)** (Power,15 kW)
WRF	150.51 (38.37 %)	13.30	13.77
Persistence	**-0.33 (-0.08 %)**	1.03	0.30
Lorenz	2.67 (0.68 %)	1.32	0.63
Diagne	-38.83 (-9.90 %)	-2.21	-3.24
Diagne (adjusted)	-6.68 (-1.70 %)	0.40	-0.36
Pelland	-15.53 (-3.96 %)	**-0.35**	-1.23
KF (daily)	-3.77 (-0.96 %)	0.72	**-0.03**

Diagne (adjusted) uses $W = 10^{-5}I$ (instead of $W = I$ in the original setting)

to illustrate the performance of measurement tracking when fluctuations occurred. All the methods generally performed well on the days that I fluctuated less. However, the Pelland and (original) Diagne models tended to over adapt in the opposite direction to the measurement trend, resulting in overall degraded performances.

V. DISCUSSION

Comparing the prediction performance between our method and the other techniques in the literature is not trivial, as (i) each post-processing method used different NWP models, (ii) the climate conditions vary in different regions, and (iii) the solar sites have different capacities. For *irradiance* forecasting performance, normalizing the RMSE by the averaged GHI can partly compensate for climate variations in different regions. Nevertheless, previous studies used different considered time periods in computing the averaged GHI, resulting in minor variations in the normalized RMSE. Here, we used the improved RMSE of the post-processing models relative to the RMSE of the baseline NWP, calculated as $100\% \times$(rmse-rmse$_{\mathrm{wrf}}$)/rmse$_{\mathrm{wrf}}$, to compare the effectiveness of the post-processing steps in the literature, while variations in the NWP implementation are controlled. Table 6 shows that our MOS+KF post-processing with a variable selection improved the baseline WRF performance by 38%, a competing progress compared to others, especially for [14], [43] that have a tropical climate close to that of Thailand.

For the solar *power* performance, most studies normalized the RMSE with a data-dependent factor (such as the mean, or the range) but computation details were not available. For example, we recommend that zero-valued observations of P from early morning or late evening should be excluded when calculating the mean; otherwise the RMSE can be too optimistically low [2, §8.3]. Thus, the compared performances shown in Table 7, were selected from studies that used the installed capacity as the normalization factor. These studies first applied a weather classification and customized each submodel to the specified weather conditions. Whereas our method does not require a prior classification step, it also achieves a comparable performance to that of [44], and our

This article has been accepted for publication in a future issue of this journal, but has not been fully edited. Content may change prior to final publication. Citation information: DOI 10.1109/ACCESS.2021.3099481, IEEE Access

TABLE 6: Examples of day-ahead solar **irradiance** prediction in literature. The improvement (%) is relative to the NWP.

Ref.	Region	Based NWP	Model	Improvement (%)
[20]	Northeastern Brazil (25 sites)	WRF	ANN	10–50
[29]	Canada (11 sites)	WRF (no spatial avg)	MOS+KF	0–22
[26]	La Reunion Island	WRF	ANN	17–18
[14]	Singapore	WRF	MOS (step-wise regression, PCA)	25–30
[43]	Singapore	WRF and WRF+data assimilation	Random forest	20–34
Our method	Central Thailand	WRF	MOS+KF	38

TABLE 7: Examples of the one-day-ahead solar **power** prediction in the literature.

Ref.	Forecasting model	Condition	NRMSE (%)
[45]	ANN	-	23.99
[46]	ANN	Clear	12.50
		Partially cloudy	24.00
		Cloudy	36.90
[44]	Wavelet+ Fuzzy ARTMAP + Firefly	Winter	12.51
		Spring	13.13
		Summer	12.11
		Fall	12.82
[47]	Wavelet+ANN	Clear	7.19
		Cloudy	16.82
		Overcast	17.61
		Rainy	19.67
Our method	MOS+KF	10 submodels	12.7-13.7

NRMSE is even 11% less than the nonlinear ANN model of [45].

From Fig. 10, our method can reduce the NRMSE from the WRF by around 7–12% during 10:00-16:00 h for both solar sites. Significant decreases were obtained from the submodels of 12:00,13:00 and 14:00 h, implying that our hypothesis is right. The main forecasting model should be split into hourly submodels in order to suitably compensate for errors from the WRF forecast, since the temporal dynamics of the weather condition throughout the day can be viewed as different hourly characteristics of solar radiation. The designed structure of containing submodels also makes the model as flexible as nonlinear ones, supported by performances reported in Tables 6 and 7. In addition to this structure, the parameter adjustment in our KF scheme provides the advantage that the model can adapt to uncertain conditions on the next day.

VI. CONCLUSION

Techniques for day-ahead forecasting of solar power generally employ an NWP model whose performance can typically be improved by a post-processing method. We implemented a KF scheme to update the parameters of the linear regression submodels; each of which predicts I at a particular time of the day. The modified KF scheme was proposed to consider the practical constraint that measurement data are limited at the time of forecasting, so the modified KF scheme was proposed. Outperforming other post-processing methods in the literature, our model achieved the NRMSE of solar power in the range of 12–13%, an additional reduction of 7-12% from the WRF performance. We also achieved a comparable performance with those of nonlinear models from previous studies, suggesting that employing simple linear models can be sufficient and are computationally cheap for real-time implementations.

Applying our method to other solar sites or with different forecasting configurations has some concerns and limitations. Our KF scheme is dependent on the forecasting specification (that forecasts must be released by 13:00 h). If users aim to apply our method with another problem statement, one has to carefully modify the KF update rule in different submodels. We also recommend that some of the initial KF parameters can be suitably tuned or input variable selection can be re-performed based on our methodology for other site locations. The limitation of relying on linear models can be extended to adaptive nonlinear models. If the nonlinearity is represented as a linear combination of nonlinear functions, it is possible to modify the KF scheme to update the weight coefficients in a similar way to our approach.

.

APPENDIX A BACKGROUND ON KF AS RECURSIVE ESTIMATION

Given a linear discrete-time stochastic system with the state $x \in \mathbf{R}^n$, output $y \in \mathbf{R}^m$, state noise w and measurement noise v, then:

$$x_{t+1} = Ax_t + w_t, \quad y_t = Cx_t + v_t, \quad t = 0, 1, 2, \ldots \quad (8)$$

This is a classical result in linear system theory that when the noises are Gaussian, the optimal prediction of x_{t+1} given the information set of measurements $Y_t = \{y_t, y_{t-1}, \ldots\}$ is the conditional mean $\mathbf{E}[x_{t+1}|Y_t]$ and can be obtained in a recursive fashion via the KF [48, §4.4], [41]. This involves two important predicted sequences and their covariances: $(\hat{x}_{t|t}, P_{t|t})$ and $(\hat{x}_{t|t-1}, P_{t|t-1})$, the pair of the optimal estimates of x_t and its covariance, conditioning on Y_t and Y_{t-1}, respectively. At time t, the KF update consists of two update steps. First, the **measurement update** utilizes the current y_t to adjust the state prediction and its covariance, where the **Kalman gain** compensates the estimation error in y_t.

$$\begin{aligned} K_t &= P_{t|t-1}C^T(CP_{t|t-1}C^T + V)^{-1}, \\ \hat{x}_{t|t} &= \hat{x}_{t|t-1} + K_t(y_t - C\hat{x}_{t|t-1}), \\ P_{t|t} &= (I - K_tC)P_{t|t-1}. \end{aligned} \quad (9)$$

Second, the **time update** (or prediction update) suggests that the optimal predicted state of time $t+1$ and its covariance progress according to the system description (8) to give (10).

$$\hat{x}_{t+1|t} = A\hat{x}_{t|t}, \quad P_{t+1|t} = AP_{t|t}A^T + W. \quad (10)$$

This article has been accepted for publication in a future issue of this journal, but has not been fully edited. Content may change prior to final publication. Citation information: DOI 10.1109/ACCESS.2021.3099481, IEEE Access

The KF scheme requires the system matrices (A, C), initial parameters: $\hat{x}_{0|-1} = x_0, P_{0|-1} = P_0$, and noise covariances W, V of w and v, respectively.

The KF can be applied to recursively update the coefficients of a linear regression model. In our context, the irradiance, as the response variable, can be explained as a linear function of a selected predictor x, given by $I = \beta_1 x_1 + \beta_2 x_2 + \beta_n x_n$. A recursive least-squares (RLS) relies on the assumption that β obeys the random walk equation:

$$\beta_{t+1} = \beta_t + w_t, \quad I_t = X_t \beta_t + v_t, \tag{11}$$

which is a time-varying version of (8) when β plays the role of the state x, I is the output y, $A = I$ and $C = X_t = (x_{1t}, x_{2t}, \ldots, x_{nt})$. Thus, at time t (when the current information of I_t is available), one can perform KF updates (9) and (10) for (11) to obtain the predicted state $\hat{\beta}_{t+1|t}$ and the predicted output $\hat{I}_{t+1} = X_{t+1}\hat{\beta}_{t+1|t}$. Since the regressor matrix at $t+1$ is needed for $\hat{I}_{t+1}$, users often select the predictors whose values at time $t+1$ can be obtained at the forecasting time t; common choices are clear-sky irradiances, solar zenith angle, or NWP weather forecasts. The user-defined covariance W suggests a degree of uncertainty about β and so its choice affects the changing rate of β_t. When one believes that the measurements are highly uncertain, V should be set sufficiently large, so that K_t in (9) becomes small, meaning less effect of output estimation error to compensate for $\hat{x}_{t|t}$ in the update.

We note that applying the KF as an RLS can be performed in different ways. First, the time index t can evolve daily or hourly and the choice can be justified upon the forecasting model specification (hour-ahead or day-ahead) that suggests about updating frequency of model coefficients. Second, the output I_t in (11) can be replaced with $e = I_{\text{nwp}} - I$, meaning that the regression model is developed for a bias correction for NWP forecasts instead of directly explaining I.

APPENDIX B MODIFIED KF

We revisit the problem of deriving a KF update of a linear time-invariant system (8), where the current measurement is available through an affine transformation. More specifically, the stated problem is to derive $\mathbf{E}[x_{t+1}|Fy_t, Fy_{t-1}, Fy_{t-2}, \ldots]$ in a KF fashion with a Gaussian assumption. The transformation F can represent several practical actions on the current measurement, *e.g.*, (i) when a measurement sensor needs a calibration, F can be regarded as a scaling matrix, (ii) when sensors of some components of y are broken, F is cast as a projection matrix, (iii) when components of y are fused, F is a row vector containing positive entries. We state this result in the following proposition.

Proposition 1. *Consider* (8) *when each of* w_t, *and* v_t *is i.i.d.*[1] *Gaussian with zero mean and covariance* W, *and* V *respectively. When* $\{Fy_s\}_{s=0}^t$ *is available, the optimal estimate of* x_t *and* y_t *in an MSE sense is obtained by the modified KF scheme.*

Measurement update:

$$\begin{aligned} K_t &= P_{t|t-1}C^T F^T (FCP_{t|t-1}C^T F^T + FVF^T)^{-1}, \\ \hat{x}_{t|t} &= \hat{x}_{t|t-1} + K_t(Fy_t - FC\hat{x}_{t|t-1}), \\ P_{t|t} &= (I - K_t FC)P_{t|t-1}. \end{aligned}$$

Time (or prediction) update:

$$\hat{x}_{t+1|t} = A\hat{x}_{t|t}, \quad P_{t+1|t} = AP_{t|t}A^T + W.$$

Proof. Firstly, we denote $Y_t = (Fy_t, Fy_{t-1}, Fy_{t-2}, \ldots, Fy_0)$ as the set of available information up to time t, we only know Fy_t, not a complete y_t. Let $\hat{x}_{t|s} = \mathbf{E}[x_t|Y_s]$ be the optimal estimate of x_t given the measurement up to time s, with the corresponding covariance of error, $P_{t|s} = \mathbf{E}[(x_t - \hat{x}_{t|s})(x_t - \hat{x}_{t|s})^T]$. When the noises w, and v are assumed to be Gaussian, the two conditioned variables: $u_1 = x_t|Y_{t-1}$ and $u_2 = Fy_t|Y_{t-1}$ are jointly Gaussian with mean: $(\hat{x}_{t|t-1}, FC\hat{x}_{t|t-1})$ and covariance

$$\begin{bmatrix} P_{t|t-1} & P_{t|t-1}C^T F^T \\ FCP_{t|t-1} & FCP_{t|t-1}C^T F^T + FVF^T \end{bmatrix} \triangleq \begin{bmatrix} \Sigma_{11} & \Sigma_{12} \\ \Sigma_{12}^T & \Sigma_{22} \end{bmatrix}. \tag{12}$$

Since (u_1, u_2) are jointly Gaussian, the conditioned variable $u_1|u_2$ is also Gaussian, with the conditional mean given by

$$\mathbf{E}[u_1|u_2] = \hat{x}_{t|t-1} + \Sigma_{12}\Sigma_{22}^{-1}(u_2 - FC\hat{x}_{t|t-1}).$$

We can also see a convenient fact that:

$$u_1|u_2 = x_t|\{Fy_t, Y_{t-1}\} = x_t|Y_t. \tag{13}$$

Therefore, the conditional mean $\mathbf{E}[x_t|Y_t]$ is given by

$$\hat{x}_{t|t} = \hat{x}_{t|t-1} + K_t(Fy_t - FC\hat{x}_{t|t-1}),$$

where K_t denotes the modified Kalman gain:

$$K_t = P_{t|t-1}C^T F^T (FCP_{t|t-1}C^T F^T + FVF^T)^{-1}.$$

From (13), the conditional covariance of $u_1|u_2$ is, in fact, $P_{t|t}$ and since $u_1|u_2$ is Gaussian, the conditional covariance is the Schur complement of the $(1,1)$ block of the matrix in (12). Hence, we arrive at the measurement update of the covariance: $P_{t|t} = P_{t|t-1} - K_t FCP_{t|t-1}$. For the prediction (or time) update, we condition the state equation (8) on Y_t:

$$x_{t+1}|Y_t = Ax_t|Y_t + w_t|Y_t = Ax_t|Y_t + w_t,$$

because w_t is uncorrelated with Y_t. Taking the expectation, we obtain $\hat{x}_{t+1|t} = A\hat{x}_{t|t}$ because w_t has zero mean. Using the description of x_{t+1} from (8), we can compute

$$\begin{aligned} P_{t+1|t} &= \mathbf{E}[(\hat{x}_{t+1|t} - x_{t+1})(\hat{x}_{t+1|t} - x_{t+1})^T] \\ &= \mathbf{E}[(A\hat{x}_{t|t} - Ax_t - w_t)(A\hat{x}_{t|t} - Ax_t - w_t)^T] \\ &= AP_{t|t}A^T + W. \end{aligned}$$

This completes the proof of the modified KF formula when the available output is $\{Fy_s\}_{s=0}^t$. □

[1] independent and identically distributed

APPENDIX C PARAMETERS IN KALMAN FILTER

From a known result of the linear regression model: $y = X\beta + e$ with p predictors and a sample size of N, an estimate of noise variance is $\hat{\sigma}^2 = \frac{1}{N-p}\|\hat{e}\|_2^2$, where $\hat{e} = y - X\hat{\beta}$, and the estimated covariance of $\hat{\beta}$ is $\mathbf{Cov}\hat{\beta} = \hat{\sigma}^2(X^TX)^{-1}$. Initialized parameters of KF applied to (6) can be explained as follows. Firstly, when the MOS model (2) is arranged in $y = X\beta$, we compute the least-squares estimate, $\hat{\beta}(t)_{\text{ls}}$ for each $t = \{t_1, t_2, \ldots, t_h\}$, and the residual error of time t is denoted by $\{e^{(d)}(t)\}_{d=1}^{N}$. Hence, the estimated variance of error term is $\hat{\sigma}^2(t) = 1/(N-p)\sum_{d=1}^{N}[e^{(d)}(t)]^2$. Then, the initial KF parameters are chosen as follows.

$$\begin{aligned}
\hat{z}^{(0|-1)} &= \begin{bmatrix}\hat{\beta}_{\text{ls}}(t_1) & \hat{\beta}_{\text{ls}}(t_2) & \cdots & \hat{\beta}_{\text{ls}}(t_h)\end{bmatrix}, \\
P^{(0|-1)} &= \mathbf{diag}(\mathbf{cov}(\hat{\beta}_{\text{ls}}(t_1)), \ldots, \mathbf{cov}(\hat{\beta}_{\text{ls}}(t_h)), \\
W &= 10^{-4}\mathbf{diag}(\hat{z}^{(0|-1)}), \\
V &= \mathbf{diag}(\hat{\sigma}^2(t_1), \hat{\sigma}^2(t_2), \ldots, \hat{\sigma}^2(t_h)).
\end{aligned}$$

The initial state variable is selected as the LS estimate of the MOS model and the covariance of state estimate is the covariance of the corresponding LS estimate. The state noise covariance is 0.01% of the magnitude of the LS estimate, meaning that the coefficients are intended to be adapted quite slowly in the KF update. The sensor noise covariance is an approximation of the residual error in the MOS model.

APPENDIX D SIGNIFICANCE TEST ON FORECASTING METRIC IMPROVEMENT

The irradiance forecasting performance indices: RMSE, MAE, and MBE from all models were tested for any significant improvement using the (non-parametric) Wilcoxon signed rank test. The null hypothesis was that $\text{metric}_{\text{other}} - \text{metric}_{\text{ours}}$ comes from a distribution with a median less than zero (the left tail test). The bold-face p-value (of less than α) in Table 8 indicates a preference for the alternative hypothesis that the metric difference has a median greater than zero, or loosely speaking, our method has a significant improvement over the other methods.

TABLE 8: The sign rank statistic and p-values of the Wilcoxon signed rank test with a significance level of 0.05.

	RMSE		MAE		MBE	
Metrics	**stat**	**p-val**	**stat**	**p-val**	**stat**	**p-val**
WRF	55	**9.77e-04**	55	**9.77e-04**	55	**9.77e-04**
Persis	55	**9.77e-04**	55	**9.77e-04**	31	3.85e-01
Lorenz	53	**2.93e-03**	55	**9.77e-04**	31	3.85e-01
Pelland	55	**9.77e-04**	55	**9.77e-04**	15	9.03e-01
Diagne	55	**9.77e-04**	55	**9.77e-04**	9	9.76e-01
Diagne (adj)	55	**9.77e-04**	55	**9.77e-04**	17	8.62e-01

As samples for running the test, we used 10 values of each metric computed in the 10-fold cross validation. The non-parametric test was adopted instead of a common t-test since the assumed normal distribution for the t-test is not known to be held with the forecasting metrics. We did not perform the significance test of solar power forecasting metrics because all the methods used the same PV conversion model,

ACKNOWLEDGMENT

This research work received financial support from the National Research Council of Thailand Fund on Renewable Energy Framework and by the Research Assistant Scholarship from Graduate School, Chulalongkorn University.

REFERENCES

[1] R. Inman, H. Pedro, and C. Coimbra, "Solar forecasting methods for renewable energy integration," *Progress in Energy and Combustion Science*, vol. 39, no. 6, pp. 535–576, 2013.

[2] J. Antonanzas, N. Osorio, R. Escobar, R. Urraca, F. M. de Pison, and F. Antonanzas-Torres, "Review of photovoltaic power forecasting," *Solar Energy*, vol. 136, pp. 78–111, 2016.

[3] M. Diagne, M. David, P. Lauret, J. Boland, and N. Schmutz, "Review of solar irradiance forecasting methods and a proposition for small-scale insular grids," *Renewable and Sustainable Energy Reviews*, vol. 27, pp. 65–76, 2013.

[4] M. Raza, M. Nadarajah, and C. Ekanayake, "On recent advances in PV output power forecast," *Solar Energy*, vol. 136, pp. 125–144, 2016.

[5] C. Wan, J. Zhao, Y. Song, Z. Xu, J. Lin, and Z. Hu, "Photovoltaic and solar power forecasting for smart grid energy management," *CSEE Journal of Power and Energy Systems*, vol. 1, no. 4, pp. 38–46, 2015.

[6] M. Akhter, S. Mekhilef, H. Mokhlis, and N. Shah, "Review on forecasting of photovoltaic power generation based on machine learning and metaheuristic techniques," *IET Renewable Power Generation*, vol. 13, no. 7, pp. 1009–1023, 2019.

[7] W. Skamarock, J. Klemp, J. Dudhia, D. Gill, D. Barker, M. Duda, X. Huang, W. Wang, and J. Powers, "A description of the advanced research WRF version 3," National Center for Atmospheric Research, Tech. Rep., 2008.

[8] P. Jiménez, J. Hacker, J. Dudhia, S. Haupt, J. Ruiz-Arias, C. Gueymard, G. Thompson, T. Eidhammer, and A. Deng, "WRF-Solar: Description and clear-sky assessment of an augmented NWP model for solar power prediction," *Bulletin of the American Meteorological Society*, vol. 97, no. 7, pp. 1249–1264, 2016.

[9] P. Jiménez, S. Alessandrini, S. Haupt, A. Deng, B. Kosovic, J. Lee, and L. Monache, "The role of unresolved clouds on short-range global horizontal irradiance predictability," *Monthly Weather Review*, vol. 144, no. 9, pp. 3099–3107, 2016.

[10] R. Perez, E. Lorenz, S. Pelland, M. Beauharnois, G. V. Knowe, K. Hemker, D. Heinemann, J. Remund, S. Müller, W. Traunmüller *et al.*, "Comparison of numerical weather prediction solar irradiance forecasts in the US, Canada and Europe," *Solar Energy*, vol. 94, pp. 305–326, 2013.

[11] V. Lara-Fanego, J. Ruiz-Arias, D. Pozo-Vázquez, F. Santos-Alamillos, and J. Tovar-Pescador, "Evaluation of the WRF model solar irradiance forecasts in Andalusia (southern Spain)," *Solar Energy*, vol. 86, no. 8, pp. 2200–2217, 2012.

[12] R. Perez and T. Hoff, "SolarAnywhere forecasting," in *Solar energy forecasting and resource assessment*, J. Kleissl, Ed. Academic Press, 2013, pp. 233–264.

[13] P. Mathiesen and J. Kleissl, "Evaluation of numerical weather prediction for intra-day solar forecasting in the continental United States," *Solar Energy*, vol. 85, no. 5, pp. 967–977, 2011.

[14] H. Verbois, R. Huva, A. Rusydi, and W. Walsh, "Solar irradiance forecasting in the tropics using numerical weather prediction and statistical learning," *Solar Energy*, vol. 162, pp. 265–277, 2018.

[15] M. Zamo, O. Mestre, P. Arbogast, and O. Pannekoucke, "A benchmark of statistical regression methods for short-term forecasting of photovoltaic electricity production, part i: Deterministic forecast of hourly production," *Solar Energy*, vol. 105, pp. 792–803, 2014.

[16] R. Verzijlbergh, P. Heijnen, S. de Roode, A. Los, and H. Jonker, "Improved model output statistics of numerical weather prediction based irradiance forecasts for solar power applications," *Solar Energy*, vol. 118, pp. 634–645, 2015.

[17] L. Massidda and M. Marrocu, "Use of Multilinear Adaptive Regression Splines and numerical weather prediction to forecast the power output of a PV plant in Borkum, Germany," *Solar Energy*, vol. 146, pp. 141–149, 2017.

[18] C. Cornaro, F. Bucci, M. Pierro, F. D. Frate, S. Peronaci, and A. Taravat, "Twenty-four hour solar irradiance forecast based on neural networks and numerical weather prediction," *Journal of Solar Energy Engineering*, vol. 137, no. 3, p. 031011, 2015.

[19] C. Cornaro, M. Pierro, and F. Bucci, "Master optimization process based on neural networks ensemble for 24-h solar irradiance forecast," *Solar Energy*, vol. 111, pp. 297–312, 2015.

[20] F. Lima, F. Martins, E. Pereira, E. Lorenz, and D. Heinemann, "Forecast for surface solar irradiance at the Brazilian Northeastern region using NWP model and artificial neural networks," *Renewable Energy*, vol. 87, pp. 807–818, 2016.

[21] A. Yona, T. Senjyu, T. Funabashi, and C. Kim, "Determination method of insolation prediction with fuzzy and applying neural network for long-term ahead PV power output correction," *IEEE Transactions on Sustainable Energy*, vol. 4, no. 2, pp. 527–533, 2013.

[22] C. Chen, S. Duan, T. Cai, and B. Liu, "Online 24-h solar power forecasting based on weather type classification using artificial neural network," *Solar Energy*, vol. 85, no. 11, pp. 2856–2870, 2011.

[23] L. Fernandez-Jimenez, A. Muñoz-Jimenez, A. Falces, M. Mendoza-Villena, E. Garcia-Garrido, P. Lara-Santillan, E. Zorzano-Alba, and P. Zorzano-Santamaria, "Short-term power forecasting system for photovoltaic plants," *Renewable Energy*, vol. 44, pp. 311–317, 2012.

[24] Y. Wu, C. Chen, and H. A. Rahman, "A novel hybrid model for short-term forecasting in PV power generation," *International Journal of Photoenergy*, vol. 2014, 2014.

[25] E. Lorenz, J. Hurka, D. Heinemann, and H. Beyer, "Irradiance forecasting for the power prediction of grid-connected photovoltaic systems," *IEEE Journal of Selected Topics in Applied Earth Observations and Remote Sensing*, vol. 2, no. 1, pp. 2–10, 2009.

[26] P. Lauret, M. Diagne, and M. David, "A neural network post-processing approach to improving NWP solar radiation forecasts," *Energy Procedia*, vol. 57, pp. 1044–1052, 2014.

[27] J. Wu and C. Chan, "Prediction of hourly solar radiation using a novel hybrid model of ARMA and TDNN," *Solar Energy*, vol. 85, no. 5, pp. 808–817, 2011.

[28] H. Glahn and D. Lowry, "The Use of model output statistics (MOS) in objective weather forecasting," *Journal of applied meteorology*, vol. 11, no. 8, pp. 1203–1211, 1972.

[29] S. Pelland, G. Galanis, and G. Kallos, "Solar and photovoltaic forecasting through post-processing of the global environmental multiscale numerical weather prediction model," *Progress in photovoltaics: Research and Applications*, vol. 21, no. 3, pp. 284–296, 2013.

[30] M. Diagne, M. David, J. Boland, N. Schmutz, and P. Lauret, "Post-processing of solar irradiance forecasts from WRF model at Reunion Island," *Solar Energy*, vol. 105, pp. 99–108, 2014.

[31] S. Haupt, B. Kosović, T. Jensen, J. Lazo, J. Lee, P. Jiménez, J. Cowie, G. Wiener, T. McCandless, M. Rogers, S. Miller, M. Sengupta, Y. Xie, L. Hinkelman, P. Kalb, and J. Heiser, "Building the Sun4Cast system: Improvements in solar power forecasting," *Bulletin of the American Meteorological Society*, vol. 99, no. 1, pp. 121–136, 2018.

[32] S. Haupt, T. McCandless, S. Dettling, S. Alessandrini, J. Lee, S. Linden, W. Petzke, T. Brummet, N. Nguyen, B. Kosović, G. Wiener, T. Hussain, and M. Al-Rasheedi, "Combining artificial intelligence with physics-based methods for probabilistic renewable energy forecasting," *Energies*, vol. 13, no. 8, p. 1979, 2020.

[33] H. Verbois, A. Rusydi, and A. Thiery, "Probabilistic forecasting of day-ahead solar irradiance using quantile gradient boosting," *Solar Energy*, vol. 173, pp. 313–327, 2018.

[34] S. Alessandrini, L. D. Monache, S. Sperati, and G. Cervone, "An analog ensemble for short-term probabilistic solar power forecast," *Applied energy*, vol. 157, pp. 95–110, 2015.

[35] S. Alessandrini and T. McCandless, "The Schaake shuffle technique to combine solar and wind power probabilistic forecasting," *Energies*, vol. 13, no. 10, p. 2503, 2020.

[36] UCAR, "User's guide for the advanced research WRF (ARW) modeling system version 3.9," https://www2.mmm.ucar.edu/wrf/users/docs/user_guide_V3/user_guide_V3.9/ARWUsersGuideV3.9.pdf.

[37] M. Iacono, J. Delamere, E. Mlawer, M. Shephard, S. Clough, and W. Collins, "Radiative forcing by long-lived greenhouse gases: Calculations with the AER radiative transfer models," *Journal of Geophysical Research: Atmospheres*, vol. 113, no. D13, 2008.

[38] S. Sobri, S. Koohi-Kamali, and N. Rahim, "Solar photovoltaic generation forecasting methods: A review," *Energy Conversion and Management*, vol. 156, pp. 459–497, 2018.

[39] D. Larson, L. Nonnenmacher, and C. Coimbra, "Day-ahead forecasting of solar power output from photovoltaic plants in the American Southwest," *Renewable Energy*, vol. 91, pp. 11–20, 2016.

[40] S. Suksamosorn, N. Hoonchareon, and J. Songsiri, "Influential variable selection for improving solar forecasts from numerical weather prediction," in *The 15th International Conference on Electrical Engineering/Electronics, Computer, Telecommunications and Information Technology (ECTI-CON)*. IEEE, 2018, pp. 333–336.

[41] B. Anderson and J. Moore, *Optimal Filtering*. Dover Publications, 2005.

[42] S. Suksamosorn, "An improvement of photovoltaic power forecasting from numerical weather prediction," Master's thesis, Chulalongkorn University, 2019.

[43] R. Huva, H. Verbois, and W. Walsh, "Comparisons of next-day solar forecasting for singapore using 3DVAR and 4DVAR data assimilation approaches with the WRF model," *Renewable Energy*, vol. 147, pp. 663–671, 2020.

[44] A. Haque, M. Nehrir, and P. Mandal, "Solar PV power generation forecast using a hybrid intelligent approach," in *2013 IEEE Power & Energy Society General Meeting*. IEEE, 2013, pp. 1–5.

[45] M. D. Giorgi, P. Congedo, and M. Malvoni, "Photovoltaic power forecasting using statistical methods: impact of weather data," *IET Science, Measurement & Technology*, vol. 8, no. 3, pp. 90–97, 2014.

[46] S. Leva, A. Dolara, F. Grimaccia, M. Mussetta, and E. Ogliari, "Analysis and validation of 24 hours ahead neural network forecasting of photovoltaic output power," *Mathematics and Computers in Simulation*, vol. 131, pp. 88–100, 2017.

[47] H. Zhu, X. Li, Q. Sun, L. Nie, J. Yao, and G. Zhao, "A power prediction method for photovoltaic power plant based on wavelet decomposition and artificial neural networks," *Energies*, vol. 9, no. 1, p. 11, 2016.

[48] P. C. Young, *Recursive estimation and time-series analysis: an introduction*. Springer Science & Business Media, 2012.

SUPACHAI SUKSAMOSORN was born in Bangkok, Thailand, in 1989. He received his B.Eng degree from Kasetsart University in 2012 and M. Eng degree from Chulalongkorn university in 2019, all in electrical engineering. He was granted a scholarship from the Electricity Generating Authority of Thailand during his master program. His research interests are in the area of smart grid and renewable energy, especially solar irradiance forecasting by numerical weather prediction.

NAEBBOON HOONCHAREON received the B.Eng. (Hons) degree in electrical engineering from Chulalongkorn University in 1993, the MS.EE and Ph.D. degrees from Purdue University in 1996 and 2000, respectively. He has joined the Faculty of Engineering, Chulalongkorn University since 2002, and has become an Associate Professor and the Head of the Department of Electrical Engineering. Currently, he has also served as a board member of Energy Conservation Fund, Ministry of Energy, Thailand; and an invited speaker for the Executive Energy Program (EEP), organized by The Institute of Industrial Energy, The Federation of Thai Industries (FTI). His research interests are in power system dynamics and control, energy management systems in Smart Grid, and solar power forecasting and applications.

JITKOMUT SONGSIRI received the B.Eng and M.Eng degrees from Chulalongkorn University in 1999 and 2002, respectively, and received the Ph.D. from University of California, Los Angeles in 2010; all in electrical engineering. She is currently an Associate Professor with the Department of Electrical Engineering, Faculty of Engineering, Chulalongkorn University, Thailand. Over the years, she has been working on statistical learning in biomedical engineering, renewable energy forecasting and numerical methods in large-scale optimization problems.